MEASUREMENT OF ENERGY DISTRIBUTION
FOR LOW POWER NANOFLARES

S.A. Bogachev (ID)
Space Research Institute, RAS,
Moscow, Russia, bogachev.sergey@gmail.com
Samara National Research University,
Samara, Russia

N.F. Erkhova (ID)
P.N. Lebedev Physical Institute, RAS,
Moscow, Russia, erhovanf@lebedev.ru

Abstract. We propose a method to measure the energy distribution of low-energy flares (nanoflares) in the energy range below 10^{23} erg. As an example, we measured the spectrum of nanoflares in the 10^{21}–10^{26} erg range for two Sun's frames observed by the SDO/AIA telescope in the 171 Å channel. Nanoflares are shown to have the power law spectrum in the 10^{22}–10^{26} erg range. The spectral index is approximately constant, i.e. energy-independent. For energies below 10^{22} erg, the spectrum begins to collapse. For lower energies, below 10^{21} erg, the method does not give statistically significant results due to major errors. The results of the study indicate that solar nanoflares can be detected up to 10^{21}–10^{22} erg energies. Results have previously been reported only for 10^{23} erg and above. The total energy flux of nanoflares in the energy range above 10^{22} erg, according to our data, is $P \approx 2 \times 10^{4}$ erg cm^{-2} s^{-1}, which is about 15 times less than heating losses of the solar corona.

Keywords: solar activity, nanoflares, coronal heating.

INTRODUCTION

The corona heating mechanism is one of the main issues in modern solar physics. In the 1980s, Parker developed a theory of hot corona formation due to low-energy flares [Parker, 1983, 1988], which drew attention to the so-called nanoflares on the Sun. The latter usually include flares with an energy from 10^{24} to 10^{27} erg, which amounts to 10^{-9}–10^{-6} of the large solar flare energy equal to 10^{33} erg (see, e.g., the review [Bogachev et al., 2020]).

The total energy released in nanoflares depends on their energy distribution. In 1991, Hudson [Hudson, 1991] suggested that this distribution follows power laws, i.e. it is described by the formula

$$N(E) = AE^{-\varphi}. \tag{1}$$

Here N is the number of nanoflares depending on their energy E; φ is the power-law distribution index; A is the multiplier determined from the normalization condition. In this case, the total energy of nanoflares within $[E_0, E_1]$ is equal to

$$P = \int_{E_0}^{E_1} AE^{-\varphi} E dE = \frac{A}{2-\varphi}\left(E_1^{2-\varphi} - E_0^{2-\varphi}\right). \tag{2}$$

According to Hudson's estimates, the corresponding energy release was $2 \cdot 10^{25}$ erg/s. At the same time, radiation losses of the quiescent solar corona occur at a rate of $\sim 6 \cdot 10^{27}$ erg/s (see, e.g., [Withbroe, Noyes, 1977]). The nanoflare energy from 10^{24} to 10^{27} erg is therefore insufficient to compensate for coronal radiation losses.

From Formula (2) it follows that if the flare spectrum is power-law with $\varphi > 2$, the main energy will be released in low-energy flares. At $\varphi < 2$, the main energy is released in large flares. At $\varphi = 2$, the energy is evenly distributed. Hudson obtained the value $\varphi \approx 1.8$.

Later on, φ was examined by a number of authors. The main results are presented in Table.

The data does not allow us to arrive at an unambiguous conclusion as to which condition is fulfilled: $\varphi > 2$ (small flares dominate over large ones) or $\varphi < 2$ (large flares dominate over small ones). Note, however, that two most recent studies based on SDO/AIA data [Ulyanov et al., 2019; Purkhart, Veronig, 2022] have obtained the value $\varphi > 2$. At the same time, the integral energy release of nanoflares in both cases turned out to be less than required for coronal heating.

Solar nanoflare spectrum measurements from 1998 to 2022

Work	Device (channel)	Energy range, erg	Power-law index φ
Berghmans et al., 1998	EIT (304, 195)	10^{24}–10^{27}	1.9, 1.35
Aschwanden et al., 2000	TRACE (171/195)	10^{24}–10^{26}	1.79
Parnell, Jupp, 2000	TRACE (171, 195)	10^{23}–10^{26}	2.4
Benz, Krucker, 2002	EIT (171/195)	10^{25}–10^{27}	2.3
Aschwanden, Parnell, 2002	TRACE (171, 195)	10^{25}–10^{27}	1.86, 1.81
Ulyanov et al., 2019	AIA (171)	10^{23}–10^{26}	2.18–2.42
Purkhart, Veronig, 2022	AIA (94, 131, 171, 193, 211, 335)	10^{24}–10^{29}	2.02–2.47

For example, Ulyanov et al. [2019] for the 10^{23}–10^{26} erg range obtained an energy release value of $9{\cdot}10^3$ erg·cm^{-2}·s^{-1}. Purkhart, Veronig [2022] got a value of $3.7{\cdot}10^4$ erg·cm^{-2}·s^{-1} for the 10^{24}–10^{29} erg range. In both cases, this appeared to be less than the corona energy losses of ~$3{\cdot}10^5$ erg·cm^{-2}·s^{-1} [Withbroe, Noyes, 1977]. In general, at $\varphi \approx 2$, the energy release weakly depends on the limits of integration.

Ulyanov et al. [2019] suggested that the missing energy can be found if the nanoflare distribution extends to the region below 10^{23} erg. They estimated that if the distribution is extended to 10^{21} erg energies, the total energy release of flares in the 10^{21}–10^{26} erg range becomes comparable to the energy the corona loses through radiation. That said, the methods for searching nanoflares adopted in [Ulyanov et al., 2019; Purkhart, Veronig, 2022] cannot detect flares in the region below 10^{23} erg because they become indistinguishable from image noise.

Zavershinsky et al. [2022] have proposed a new method for detecting nanoflares, which cannot measure the energy of each individual nanoflare, but can estimate the total number of flares even in the region of very low energies. Using this method, the authors, for instance, came to a conclusion about the uniform spatial distribution of nanoflares over heliographic latitudes, which significantly distinguishes them from ordinary flares observed in activity belts. We suppose that this method can also be used to estimate the shape of the nanoflare energy distribution in the region of very low energies, undetectable by other methods.

In this paper, we conduct such a study and report its results. The structure of the paper is as follows. Section 1 lists the observational data we use and briefly outlines the processing method. Section 2 presents the results. Section 3 contains discussion and conclusions.

1. DATA AND METHOD

Nowadays, the main source of data for detecting nanoflares is high-resolution images of the solar corona in the vacuum UV spectral region (~100 Å). Nanoflares in such images are observed as a local burst often occurring in just one pixel (sometimes in several adjacent pixels) of the image and lasting for no more than a few tens of seconds. We have used data acquired by the AIA telescope [Lemen et al., 2012] on board the Solar Dynamics Observatory (SDO) in the 171 Å channel.

The SDO/AIA telescope provides full-disk solar images of size 4096×4096 pixels with an angular resolution of 0.6″ per pixel and a cadence of 12 s. The radiation in the 171 Å channel is formed mainly by the FeIX iron spectral line at a temperature of ~$0.6^{10.6}$ K, which is in good agreement with the plasma temperature in solar nanoflares.

For the study, we have selected two solar regions (Figure 1). The corresponding series of images was captured by SDO/AIA on May 20, 2019 at 12:00–13:00 UT. The number of images in the series is 300, the size of the regions is 512×512 pixels. The regions are located
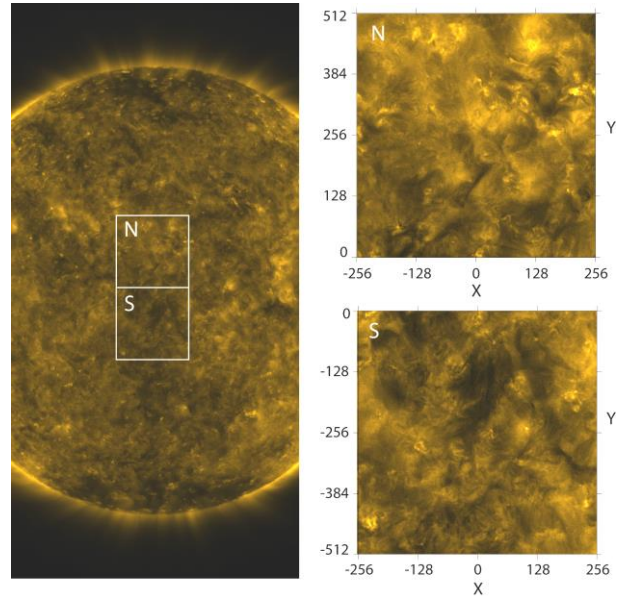

Figure 1. Quiet-Sun regions studied in the work: N — northern region, S — southern region

symmetrically about the center of the apparent solar disk in the northern and southern hemispheres. The main difference between the regions was the different brightness of the solar disk: the northern region had a slightly higher brightness than the southern one. We found it useful to test the method in different conditions. In other respects, the observation period was chosen relatively randomly since the main purpose of the work was to explore the fundamental possibility of detecting very low energy nanoflares, and not to study a specific period or region on the Sun.

Treating space telescope data often requires additional image processing, specifically, reduction of jitter, reduction of differential rotation of the Sun, consideration of the inhomogeneous sensitivity of the detector (flat field function), as well as elimination of spikes arising from energetic particles and the signal in bad pixels in the image. Since we used Level 1 AIA data, a flat field correction had been made in the data, as well as bad pixels and spikes arising from energetic particles had been removed. We controlled the position of the Sun's center, using FITS header data. According to the data, there was no jitter or it was previously reduced. This was also confirmed by visual examination of images. We also neglected the differential rotation of the Sun since the characteristic duration of the events under study was 12 s, and the maximum image shift over such a period was less than 0.06 of pixel size. In general, we came to the conclusion that the pre-processing of level 1 images is sufficient for our study and no additional processing is required. Additional image processing was not made either in [Zaverchinsky et al., 2022]. Purkhart, Veronig [2022] reduced only the differential rotation, as they dealt with longer events.

Below, we describe the data analysis method for the northern region. For the southern region, the data was analyzed in the same way. For it, we present only the final result here.

Following the method described in [Zavershinsky et al., 2022], we transformed series of images into a data cube $I_i(x, y)$, where i is the image number from 1 to 300; x, y are pixel coordinates (from 1 to 512). Next, we calculated the difference

$$DI_i(x, y) = I_{i+1}(x, y) - I_i(x, y). \qquad (3)$$

The value of $DI_i(x, y)$ is thus equal to the change (increase/decrease) of a signal in pixel (x, y) when going from i to $i+1$.

In the absence of flares and other manifestations of activity, the main cause for the signal change in AIA images is photon noise. Thus, we can assume that the DI array will have a normal (Gaussian) distribution with a near-zero mean and a variance σ proportional to $\sim I^{0.5}$. From information on calibration of the SDO/AIA telescope [Boerner et al., 2012], Zavershinsky et al. [2022] have determined the theoretical dependence $\sigma(I)$ for the 171 Å channel

$$\sigma(I) \approx 1.08 I^{0.5} \qquad (4)$$

and have shown that it fits the experimental value well

$$\sigma(I) \approx 1.06 I^{0.52}. \qquad (5)$$

While Formulas (4) and (5) are almost identical, the experimental distribution cannot completely coincide with the theoretical one since DI changes occur not only due to photon noise, but also due to real physical processes affecting the radiation. In particular in the quiescent solar corona in the absence of large flares or other significant manifestations of activity, nanoflares should have a significant impact on the shape of the DI distribution.

According to experimental data, the energy distribution of nanoflares follows power laws. That is why the difference between the DI spectrum and the Gaussian form must be especially noticeable at large values of DI, where the power-law distribution dominates over the exponential one. We interpret the corresponding difference between the Gaussian distribution generated by noise and the actual distribution obtained from data processing as a possible contribution of low-energy events.

To determine this contribution, we divided the range into intervals of 10 measurements, for each interval we found the DI function from Formula (3), and then we constructed the corresponding normal Gaussian distribution and the actual distribution. We deal with a signal range from 130 to 320 since a preliminary study has shown that for this region on the Sun the range contains more than 90 % of all events. Significant statistical errors occur outside of this range due to the small number of events.

An example of the processing (for the intensity from 200 to 210 measurements) is given in Figure 2. In fact, the measured DI values in this intensity range were within $\sim\pm100$ measurements. The theoretical value of the variance for this range, derived from Formula (4), $\sigma(I)=15.46$. The actual value $\sigma(I)=16.28$. Region I shows a normal (Gaussian) distribution for $\mu=0$ and $\sigma=15.46$. The distribution is normalized to the total

number of events in the range from 200 to 210. Region II reveals the actual distribution, i.e. the experimental number of events detected in the corresponding range of values.

The measurement error shown in Figure 2 was defined as a superposition of the statistical error and the error caused by the measurement resolution. We considered the latter to be equal to 1/5 since the DI distribution was constructed with increment of 5 measurements. Thus,

$$err = \sqrt{\left(\sqrt{n}\right)^2 + 0.2^2}, \qquad (6)$$

where n is the number of events in the interval.

As expected, the most significant discrepancy between the noise distribution and the actual distribution is observed in the region of large DI values. Specifically, for $DI>70$ (corresponds to a level of $\sim4.5\sigma$), only 16 events must have been observed for the noise distribution (region I). In fact, 149 events have been detected in this region (region II).

The difference between the actual distribution (region II) and the noise distribution (region I) is illustrated in Figure 3. Note that at $DI<30$ measurement errors become comparable to the measured values. A similar situation is observed at $DI>85$, but for some other reason — because of the small number of events in this region.

The corresponding procedure was performed for all intervals in the intensity range from 130 to 320 (recall that Figures 2, 3 present the results only for the interval 200–210). Further, we summed all distributions and obtained the integral distribution for the entire range of I values. The corresponding distributions for the northern and southern regions of the Sun, as well as their normalization, are discussed in Section 2.
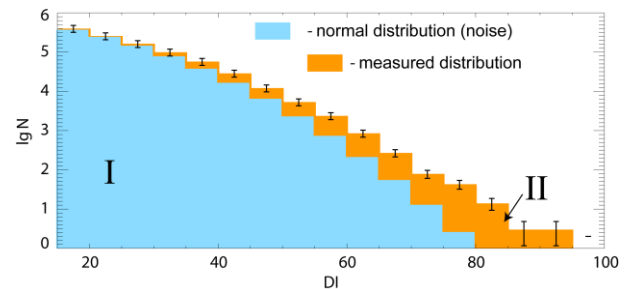

Figure 2. Image processing: region I is a normal signal distribution corresponding to noise; region II is the actual distribution measured in the image
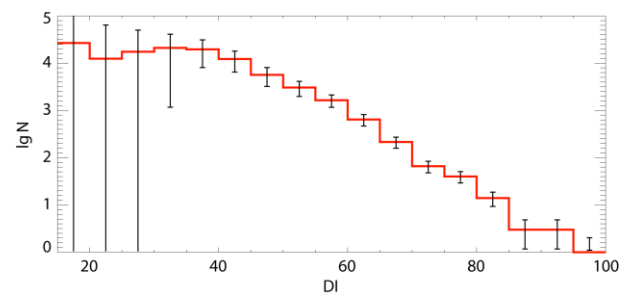

Figure 3. Difference between the actual distribution (region II in Figure 2) and the normal distribution (region I in Figure 2)

2. RESULTS

Figure 4 plots the integral distribution of all events exceeding the noise level for the northern region of the Sun. The values of N (Y-axis) are reduced to the units of number of events·cm^{-2}·s^{-1}. As already noted, low-energy flares, according to present-day views, have a power-law distribution, which is described by Formula (1). In the logarithmic representation, the power-law function is transformed into a linear one:

$$\lg N = \lg A - \varphi \lg E. \qquad (7)$$

According to Figure 4, the distribution $N(DI)$ follows power laws in the DI range from ~50 to 150 (in logarithmic representation from ~1.7 to 2.2). At $DI<50$, the diagram deviates from the power-law dependence. Such a power-law break at low energies is common for nanoflare distributions (see, e.g., [Ulyanov et al., 2019; Purkhart, Veronig, 2022]) and is associated with the inability to detect nanoflares below the sensitivity threshold depending on the chosen method. In the two works mentioned above, the threshold was set at a level 5σ because below this level the method adopted could not distinguish individual nanoflares from noise. In this work, we apply a different principle — the total number of events is recorded instead of individual nanoflares; for this reason, we believe that this threshold can be shifted to lower energies.

In order to compare the obtained distribution with those derived by other authors, we have calibrated the diagram in Figure 4 to reduce $N(DI)$ to $N(E)$, i.e. to the energy (E) dependence. First of all, since the distribution of $N(DI)$ follows power laws, as does the distribution of $N(E)$, we assume that the DI measurements and the energy E are related by

$$DI = BE^b. \qquad (8)$$

Only in this case, the distribution during the transformation will continue to follow power laws.

The power-law part of the diagram in Figure 4 is described by the formula

$$N = C(DI)^{-c}. \qquad (9)$$

According to Figure 4, $C=10^{-4.92\pm0.24}$, $c=-9.06\pm0.12$.

In this case, by comparing Formulas (1) and (9), we can write

$$dN = C\left(DI\right)^{-c} d\left(DI\right) = AE^{-\varphi}dE. \qquad (10)$$

Hence, in view of (8), we get:

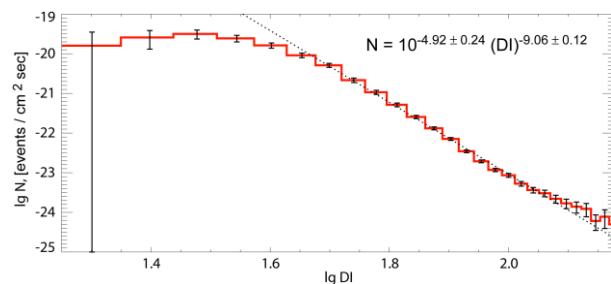$$CB^{1-c}bE^{-(cb+1-b)} = AE^{-\varphi}. \qquad (11)$$

Figure 4. Integral experimental distribution of low-energy events $N(DI)$ measured for the northern region of the Sun

Thus,

$$A = CB^{1-c}b, \qquad (12)$$

$$\varphi = cb + 1 - b. \qquad (13)$$

For normalization, we use the work [Ulyanov et al., 2019], where the energy distribution of nanoflares in the energy range from 10^{23} to 10^{25} erg has been constructed in the same channel 171 Å of the SDO/AIA telescope under similar conditions of solar minimum. The distribution shape in [Ulyanov et al., 2019] was as follows (we have converted it into a format convenient for us)

$$N = 10^{7.4} E^{-2.18\pm0.2} \left[\text{events cm}^{-2}\ \text{s}^{-1} \right]. \qquad (14)$$

Hence, $A=10^{7.4}$, $\varphi=2.18\pm0.2$. The error for the multiplier A in [Ulyanov et al., 2019] is omitted. Thus, (12) and (13) yield:

$$b = \frac{\varphi-1}{c-1} = 0.146, \qquad (15)$$

$$\lg B = \frac{\lg A - \lg C - \lg b}{1-c} = -1.63. \qquad (16)$$

According to (8), we derive a formula for renormalizing the X-axis of the diagram in Figure 4:

$$\lg E = \frac{1}{2}\left(\lg DI - \lg B\right) = 6.81\lg DI + 11.2. \qquad (17)$$

The renormalization for the Y-axis can be found from the relation

$$N(E)dE = N(DI)d(DI). \qquad (18)$$

In the literature, the spectrum of nanoflares is usually constructed not in units of number of event·cm^{-2}·s^{-1}, but in energy flux units P erg·cm^{-2}·s^{-1}. The relationship between $P(E)$ and $N(E)$ is determined as follows

$$P(E) = EN(E). \qquad (19)$$

Passing from N to P, Formula (18) can be written as

$$P(E)dE = EN(DI)d(DI). \qquad (20)$$

Substituting (8) into (18), we obtain the desired normalization condition for the Y-axis of the diagram in Figure 4:

$$\lg P(E) = \lg N(DI) + \lg(DI) + \lg b. \qquad (21)$$

The result — a diagram transformed from $N(DI)$ to $P(E)$ — is presented in Figure 5. For comparison, we have plotted the distribution from [Ulyanov et al., 2019] on it (see Figure 7 therein).

Figure 6 demonstrates the spectrum obtained in the same way for the southern region of the Sun.

3. DISCUSSION AND CONCLUSIONS

The issue concerning the presence of very low-energy flares on the Sun below 10^{23} erg is still debatable. Modern observations with SDO/AIA telescopes cannot confidently identify events in this range since their amplitude turns out to be comparable to the amplitude of photon noise. At the same time, the presence or absence of such events is essential for the problem of corona heating, as the total energy of nanoflares in the region of interest (above 10^{23} erg) is not
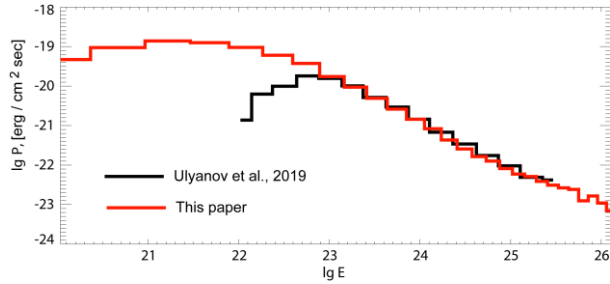
Figure 5. Distribution of energy flux $P(E)$ associated with nanoflares as measured for the northern region of the Sun
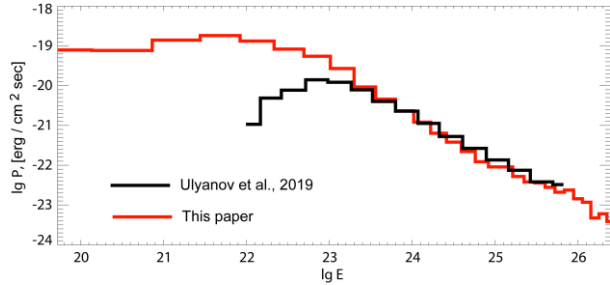

Figure 6. The same for the southern region of the Sun

enough to fully compensate for coronal radiation losses. That is why, objects of other types with low energy release are currently widely studied, such as microflares [Kirichenko, Bogachev, 2013; Kirichenko, Bogachev, 2017; Mitra-Kraev, Del Zanna, 2019; Li et al., 2022], bright points [Ulyanov et al., 2010], spicules and macrospicles [Loboda, Bogachev, 2015, 2017, 2019; Cho et al., 2019; Shimojo et al., 2020], as well as high-temperature plasma sources, both small-sized (for example, X-ray points [Reva et al., 2012, 2018; Madjarska, 2019]) and large high-temperature regions formed during flares and in the quiescent solar corona [Grechnev et al., 2006]. The possibility of plasma heating during coronal mass ejections is also discussed exhaustively [Murphy et al., 2011; Reva et al., 2022].

However, the simplest solution to this problem cannot be ruled out, namely, the search for flares of even lower energy, a large number of which can at least partially solve the problem of missing energy for corona heating.

In this paper, we have explored the possibility of statistically distinguishing minor events (nanoflares) from photon noise in SDO/AIA images in the 171 Å line. We proceeded from the fact that the nanoflare distribution, according to some authors, follows power laws and hence, starting from a threshold, should dominate over the noise distribution. We borrowed this assumption from [Zavershinsky et al., 2022]. To solve this problem, we have analyzed two regions of the quiet Sun observed by SDO/AIA during solar minimum in May 2019. In both cases, we did find a discrepancy between the theoretical distribution for photon noise and the actual signal distribution. The difference between the distributions follows power laws, i.e. it corresponds to the expected distribution of low-energy solar flares. We have developed a method for calibrating the spectrum by comparing it with nanoflare distributions obtained by other authors. As a comparison spectrum, we chose the nanoflare distribution from [Ulyanov et al., 2019],

measured in November 2010. The spectrum was taken in the same range of 171 Å we dealt with, as well as under similar conditions — near solar minimum.

Preliminary results of the study (Figures 5, 6 for different solar regions) show that the contribution of low-energy flares can be traced to at least ~10^{22} erg, which is about by an order of magnitude lower than the threshold to which nanoflares are detected by methods based on searching for individual events. In the energy range below 10^{22} erg, a power-law break takes place; this means that either at such energies the number of nanoflares begins to decrease or the accuracy of the method becomes insufficient.

According to our data, the total nanoflare energy flux in the range from 10^{22} to 10^{26} erg $P \approx 2 \cdot 10^4$ erg cm^{-2} s^{-1}. Note that this is still not enough to compensate for radiative losses of the solar corona, which amount to $3 \cdot 10^5$ erg cm^{-2} s^{-1} [Withbroe, Noyes, 1977].

Nevertheless, we believe that the method proposed in this work is promising and also preliminarily confirms the possibility of detecting solar nanoflares up to 10^{22} erg. According to our results, the spectrum slope of nanoflares in the energy range from 10^{22} to 10^{23} erg does not change and coincides with that in the range from 10^{23} to 10^{26} erg. We deem this fact important for the ongoing discussion about preservation of the flare spectrum shape in the low-energy region or formation of a break there.

REFERENCES

Aschwanden M.J., Parnell C.E. Time variability of the "Quiet" sun observed with TRACE. II. Physical parameters, temperature evolution, and energetics of extreme-ultraviolet nanoflares. *Astrophys. J.* 2000, vol. 535, no. 2, p. 1047. DOI: 10.1086/308867.

Aschwanden M.J., Parnell C.E. Nanoflare statistics from first principles: fractal geometry and temperature synthesis. *Astrophys. J.* 2002, vol. 572, no. 2, p. 1048. DOI: 10.1086/340385.

Benz A.O., Krucker S. Energy distribution of microevents in the quiet solar corona. *Astrophys. J.* 2002, vol. 568, no. 1, p. 413. DOI: 10.1086/338807.

Berghmans D., Clette F., Moses D. Quiet Sun EUV transient brightenings and turbulence. A panoramic view by EIT on board SOHO. *Astronomy and Astrophysics.* 1998, vol. 336, pp. 1039–1055.

Boerner P., Edwards C., Lemen J., Rausch A., Schrijver C., Shine R., et al. Initial calibration of the atmospheric imaging assembly (AIA) on the solar dynamics observatory (SDO). *Solar Phys.* 2012, vol. 275, pp. 41–66. DOI: 10.1007/s11207-011-9804-8.

Bogachev S.A., Ulyanov A.S., Kirichenko A.S., Loboda I.P., Reva A.A. Microflares and nanoflares in the solar corona. *Physics-Uspekhi.* 2020, vol. 63, no. 8, p. 783. DOI: 10.3367/UFNe.2019.06.038769.

Cho I.H., Moon Y.-J., Cho K.-S., Nakariakov V.M., Lee J-Y, Kim Y-H. A new type of jet in a polar limb of the solar coronal hole. *Astrophys. J. Lett.* 2019, vol. 884, no. 2, p. L38. DOI: 10.3847/2041-8213/ab4799.

Grechnev V.V., Kuzin S.V., Urnov A.M., Zhitnik I.A., Uralov A.M., Bogachev S.A., et al. Long-lived hot coronal structures observed with CORONAS-F/SPIRIT in the Mg XII line. *Solar System Res.* 2006, vol. 40, no. 4, pp. 286–293.

Hudson H.S. Solar flares, microflares, nanoflares, and coronal heating. *Solar Phys*. 1991, vol. 133, no. 2, pp. 357–369. DOI: 10.1007/BF00149894.

Kirichenko A.S., Bogachev S.A. Long-duration plasma heating in solar microflares of X-ray class A1. 0 and lower. *Astronomy Letters*. 2013, vol. 39, no. 11, pp. 797–807. DOI: 10.1134/ S1063773713110042.

Kirichenko A.S., Bogachev S.A. Plasma heating in solar microflares: Statistics and analysis. *Astrophys. J*. 2017, vol. 840, no. 1, p. 45. DOI: 10.3847/1538-4357/aa6c2b.

Lemen J.R., Title A.M., Akin D.J., Boerner P.F., Chou C., Drake J.F., et al. The Atmospheric Imaging Assembly (AIA) on the Solar Dynamics Observatory (SDO). *Solar Phys*. 2012, vol. 275, pp. 17–40. DOI: 10.1007/s11207-011-9776-8.

Li Z., Su Y., Veronig A.M., Kong S., Gan W., Chen W. Detailed thermal and nonthermal processes in an A-class microflare. *Astrophys. J*. 2022, vol. 930, no. , p. 147. DOI: 10.3847/1538-4357/ac651c.

Loboda I.P., Bogachev S.A. Quiescent and eruptive prominences at solar minimum: a statistical study via an automated tracking system. *Solar Phys*. 2015, vol. 290, no. 7, pp. 1963–1980. DOI: 10.1007/s11207-015-0735-7.

Loboda I.P., Bogachev S.A. Plasma dynamics in solar macrospicules from high-cadence extreme-UV observations. *Astronomy and Astrophysics*. 2017, vol. 597, p. A78. DOI: 10.1051/0004-6361/201527559.

Loboda I.P., Bogachev S.A. What is a macrospicule? *Astrophys. J*. 2019, vol. 871, no. 2, p. 230. DOI: 10.3847/1538-4357/aafa7a.

Madjarska M.S. Coronal bright points. *Living Reviews in Solar Physics*. 2019, vol. 16, no. 1, pp. 1–79. DOI: 10.1007/s41116-019-0018-8.

Mitra-Kraev U., Del Zanna G. Solar microflares: a case study on temperatures and the Fe XVIII emission. *Astronomy and Astrophysics*. 2019, vol. 628, p. A134. DOI: 10.1051/0004-6361/201834856.

Murphy N.A., Raymond J.C., Korreck K.E. Plasma heating during a coronal mass ejection observed by the solar and heliospheric observatory. *Astrophys. J*. 2011, vol. 735, no. 1, p. 17. DOI: 10.1088/0004-637X/735/1/17.

Parker E.N. Magnetic neutral sheets in evolving fields. I-General theory. *Astrophys. J*. 1983, vol. pp. 635–647. DOI: 10.1086/160636.

Parker E.N. Nanoflares and the solar X-ray corona. *Astrophys. J*. 1988, vol. 330, pp. 474–479. DOI: 10.1086/166485.

Parnell C.E., Jupp P.E. Statistical analysis of the energy distribution of nanoflares in the quiet Sun. *Astrophys. J*. 2000, vol. 529, no. 1, p. 554. DOI: 10.1086/308271.

Purkhart S., Veronig A.M. Nanoflare distributions over solar cycle 24 based on SDO/AIA differential emission measure observations. *Astronomy and Astrophysics*. 2022, vol. 661, p. A149. DOI: 10.1051/0004-6361/202243234.

Reva A., Shestov S., Bogachev S., Kuzin S. Investigation of hot X-ray points (HXPs) using spectroheliograph Mg XII experiment data from CORONAS-F/SPIRIT. *Solar Phys*. 2012, vol. 276, no. 1, pp. 97–112. DOI: 10.1007/s11207-011-9883-6.

Reva A., Ulyanov A., Kirichenko A., Bogachev S., Kuzin S. Estimate of the upper limit on hot plasma differential emission measure (DEM) in non-flaring active regions and nanoflare frequency based on the Mg xii spectroheliograph data from CORONAS-F/SPIRIT. *Solar Phys*. 2018, vol. 293, no. 10, pp. 1–15. DOI: 10.1007/s11207-018-1363-9.

Reva A.A., Bogachev S.A., Loboda I.P., Ulyanov A.S., Kirichenko A.S. Observations of current sheet heating in X-ray during a solar flare. *Astrophys. J*. 2022, vol. 931, no. 2, p. 93. DOI: 10.3847/1538-4357/ac6b3d.

Shimojo M., Kawate T., Okamoto T.J., Yokoyama T., Narukage N., Sakao T., et al. Estimating the temperature and density of a spicule from 100 GHz data obtained with ALMA. *Astrophys. J. Lett*. 2020, vol. 888, no. 2, p. L28. DOI: 10.3847/2041-8213/ab62a5.

Ulyanov A.S., Bogachev S.A., Kuzin S.V. Bright points and ejections observed on the sun by the KORONAS-FOTON instrument TESIS. *Astronomy Rep*. 2010, vol. 54, no. 10, pp. 948–957. DOI: 10.1134/S1063772910100082.

Ulyanov A.S., Bogachev S.A., Reva A.A., Kirichenko A.S., Loboda I.P. The energy distribution of nanoflares at the minimum and rising phase of solar cycle 24. *Astronomy Lett*. 2019, vol. 45, no. 4, pp. 248–257. DOI: 10.1134/S1063 773719040078.

Withbroe G.L., Noyes R.W. Mass and energy flow in the solar chromosphere and corona. *Ann. Rev. Astron. Astrophys*. 1977, vol. 15, pp. 363–387. DOI: 10.1146/annurev.aa.15.090177. 002051.

Zavershinsky D.I., Bogachev S.A., Belov S.A., Ledentsov L.S. Method for searching nanoflares and their spatial distribution in the solar corona. *Astronomy Lett*. 2022, vol. 48, no. 9. (In print).